Analysis of the Composite Material Behaviour Subjected to Dynamic Bending using the Hopkinson Bar

Abdellah MASSAQ[1,2], Alexis RUSINEK[3], Maciej KLÓSAK[4,5],
Abdellah BOULOUZ[2], Lahcen KOUTTI[2]

[1] *Ecole Nationale des Sciences Appliquées*
Laboratory OSCARS
Avenue Abdelkrim Khattabi, 40000, Guéliz-Marrakech, Morocco

[2] *Ibn Zohr University – Faculty of Sciences Agadir*
Laboratory LABSIV
BP. 8106 Quartier Dakhla, Agadir, Morocco
e-mail: a.massaq@uiz.ac.ma

[3] *National Engineering School of Metz ENIM*
Laboratory of Mechanics, Biomechanics, Polymers and Structures – LaBPS, EA 4632
1 route d'Ars Laquenexy, CS 65820 57078 METZ Cedex 3, France
e-mail: rusinek@enim.fr

[4] *Universiapolis, Ecole Polytechnique d'Agadir*
Bab Al Madina, Quartier Tilila, Agadir, Morocco
e-mail: klosak@e-polytechnique.ma

[5] *The International University of Logistics and Transport in Wrocław*
Sołtysowicka 19B, 51-168 Wrocław, Poland

The aim of this study is to propose an experimental approach supported by an analytical analysis for polymer materials under dynamic loading. The experimental technique of Hopkinson split pressure bar is used which allows for high impact velocities. The specimens are subjected to the three-point bending and the efficiency of the experimental technique is proved. During quasi-static and dynamic bending tests, the rupture mode is described and the evolution of the energy and the ultimate stresses as a function of the initial impact velocity is discussed. In addition, the critical impact velocity estimated above an important change in the rupture mode is observed.

In order to better describe the physical phenomena encountered during the three-point bending impact, the analysis is supported by a rheological model based on a mass-spring system.

Key words: impact velocity, three-point bending, woven composite, dynamic behaviour, shock, Hopkinson bar.

1. Introduction

Thermoplastic composites such as the woven glass-fibre-reinforced Polyamide 6 (PA6) are breakthrough materials in different industrial sectors due to their mechanical properties. This type of material keeps its mechanical performances because the matrix transfers the loading from one fibre to another and thus a sufficient connection between fibres is retained. It is important to determine the type of reinforcement for optimal resistance to traction, bending and impact. For many years this material has been gaining a commercial success due to its excellent thermal, electrical and mechanical properties coupled with remarkable tribological performances. In many applications there are high requirements concerning rigidity, dimensional stability and heat deflection temperature and PA6 satisfies them satisfactorily. It should be noted that the anisotropy of this material is mainly due to fibre orientation and it may cause the element warping, however, the use of PA6 has received good reviews in several industrial applications.

The practical interest in using a bending test lies in the specimen geometry which is relatively simple and well known in the industrial environment. In general, a bending test cannot provide satisfactory information about a rupture by measuring the forces. The waves induced by bending are relatively low and specimen vibrations generate many perturbations. One solution is to use the Hopkinson bar system [1] which allows to eliminate some of these problems, especially in terms of obtaining a better quality of measurements.

Behaviour of the woven glass-fibre-reinforced Polyamide 6 under dynamic loading is studied. A new technique is used [1] offering a big advantage of high impact velocities up to 200 m/s which are by far higher compared to the ones in Charpy tests [2, 3], which are limited to 5 m/s. A Hopkinson bar system [4] has been chosen to eliminate certain problems encountered during dynamic tests and to ensure the accuracy of measurement results. The proposed test configuration uses a Hopkinson set-up without an input bar (direct impact) allowing to eliminate the loading time between the incident and transmitted wave.

The new configuration allows to measure not only the applied force, but also the displacement of the loading point, using immediate measurements.

The results gathered from the study are compared to the results obtained from the dynamic modelling of the mass-spring system under shock.

2. Composite specimen and test description

2.1. Composite specimen

Dynamic bending tests are performed using the woven glass-fibre-reinforced Polyamide 6 (PA6) with a stacking sequence of $0°/90°$. The tests have been

realised with parallelepiped specimens without notches. External and internal faces of the specimens are neither treated nor rectified in order not to induce any additional surface defaults. The size of the specimen is presented in Fig. 1. In order to reduce the effect of inertial forces on the measurements of the force transmitted at high impact velocities, a specimen with high stiffness geometry has been used, characterised by the ratio S/W equal to 4.5 where S is the specimen span (distance between supports) and W is its height. The specimens are loaded perpendicularly to the fibres.
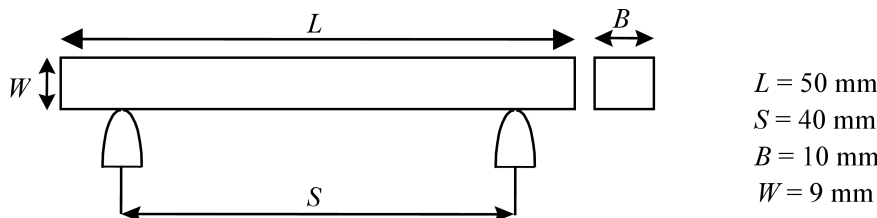
FIG. 1. Specimen geometry and schematic description of the device used for bending tests.

The material characteristics are the dynamic Young modulus, determined by the statistic method [5], of the order of 10.098 GPa and the volume mass is $\rho = 1834$ kg/m^3.

2.2. Test description

The test assembly used in this study has been initially proposed by MAS-SAQ *et al.* [1]. The dynamic bending is performed using a system of Hopkinson bars. The direct impact is applied without an input bar, therefore the projectile directly hits the specimen. The impact velocity is measured by the photodiodes fixed at the end of the tube, Fig. 2. The assembly is composed of one tube (Fig. 2) instead of two output bars as it was proposed by many authors [14–20]. This improvement allows to minimise vibrations of Pochhammer-
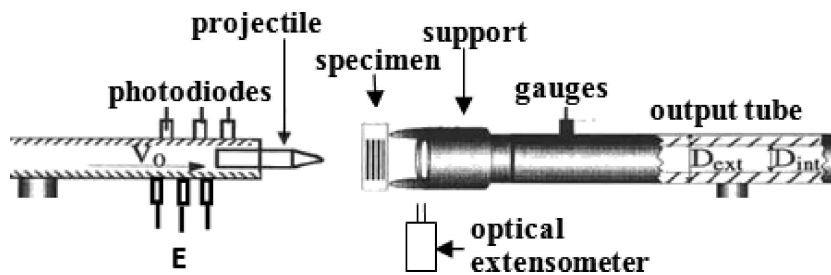
FIG. 2. Configuration for dynamic bending test [1].

Chree type which are registered during the impact. The radial inertia is by far smaller in the tube than in the plain bar of the same external diameter [6–7]. In fact, the radial dispersions are shared by external and internal parts of the tube.

The gauges are glued to the output tube in order to detect a signal of the axial force transmitted through the specimen, which is done by measuring the wave of the transmitted longitudinal deformation $\varepsilon_T(t)$. The impact end of the projectile has a bevelled form of the length L_b and the projectile length is L_p. The geometrical characteristics of the machine configuration are given in Table 1.

Table 1. Characteristics of the projectile and the tube.

Projectile length	$L_p = 100$ mm
Length of the conic part of the projectile	$L_b = 30$ mm
Projectile diameter	$D = 22$ mm
Projectile mass	$m = 215$ g
Tube length	$L_h = 4000$ mm
Internal diameter of the tube	$D_{\text{int}} = 30$ mm
External diameter of the tube	$D_{\text{ext}} = 50$ mm

The measurement of the specimen displacement is facilitated by the use of the efficient optical extensometer (Zimmer type) which follows the specimen movement without contact.

The equation to calculate the support reaction is expressed by

$$(2.1) \qquad F(t) = \frac{\pi}{4}(D_{\text{ext}}^2 - D_{\text{int}}^2) \cdot E_{\text{tub}} \cdot \varepsilon_T(t),$$

where E_{tub} is Young's modulus of the tube, and D_{ext} and D_{int} are, respectively, the external and internal diameters of the Hopkinson tube.

The real displacement of the central point of the tensile face of the specimen δ_s is given by

$$(2.2) \qquad \delta_s(t) = \delta_{\text{ext}}(t) - \delta_{\text{tub}}(t),$$

where δ_{ext} and δ_{tub} represent, respectively, the displacement measured by the optical extensometer and the elastic displacement of the Hopkinson tube due to impact.

The analysis of the elastic waves propagation in the bars or in the tubes allows to determine the elastic tube displacement δ_{tub} as a function of the

transmitted wave $\varepsilon_T(t)$. Thus, the value of δ_{tub} is expressed by the following equation:

$$(2.3) \qquad \delta_{\text{tub}}(t) = C_0 \int_0^t \varepsilon_T(\xi) \mathrm{d}\xi.$$

The combination of Eqs. (2.2) and (2.3) gives the real deflection at the central point of the specimen:

$$(2.4) \qquad \delta_s(t) = \delta_{\text{ext}}(t) - C_0 \int_0^t \varepsilon_T(\xi) \mathrm{d}\xi.$$

The wave celerity C_0 of the elastic wave propagating in the tube is defined by

$$(2.5) \qquad C_0 = \sqrt{E_{\text{tub}}/\rho_{\text{tub}}}$$

with ρ_{tub} being the volume mass density of the tube.

The fundamental dynamic law applied to the specimen subjected to the three-point bending gives:

$$(2.6) \qquad F_I - F_T = m_s \cdot \ddot{\delta}_s,$$

where F_I is the force applied at the impact point of the specimen, m_s is the specimen mass, F_T is the sum of support reactions given by Eq. (2.1), δ_s represents the deflection measured at the specimen centre defined by Eq. (2.4).

3. Experimental results

3.1. Quasi-static tests

Figure 3 shows a set of force-displacement curves, obtained under quasi-static conditions of loading, realised by different displacement rates. The first part of all curves reveals an elastic linear behaviour, up to approximately 70% of the total loading. Above this limit, we observe a decrease in rigidity. This transition is a result of the specimen cracking, and – to be more precise – this is due to the matrix micro-cracking (see Fig. 4). This microcracks, in the matrix, take place at the tensile face of the specimen, in the area of the maximum stress which confirms the rupture in pure tension (see Fig. 5a). Then the curve reaches its maximum. The peak value corresponds to the rupture of the fibres located in the proximity of the tensile face and therefore reflects the appearance of macroscopic cracks. Once the maximum value is reached, the specimen loses all its rigidity which tends to zero. The deflection increases and the process of extracting of broken fibres takes place (see Fig. 5b).
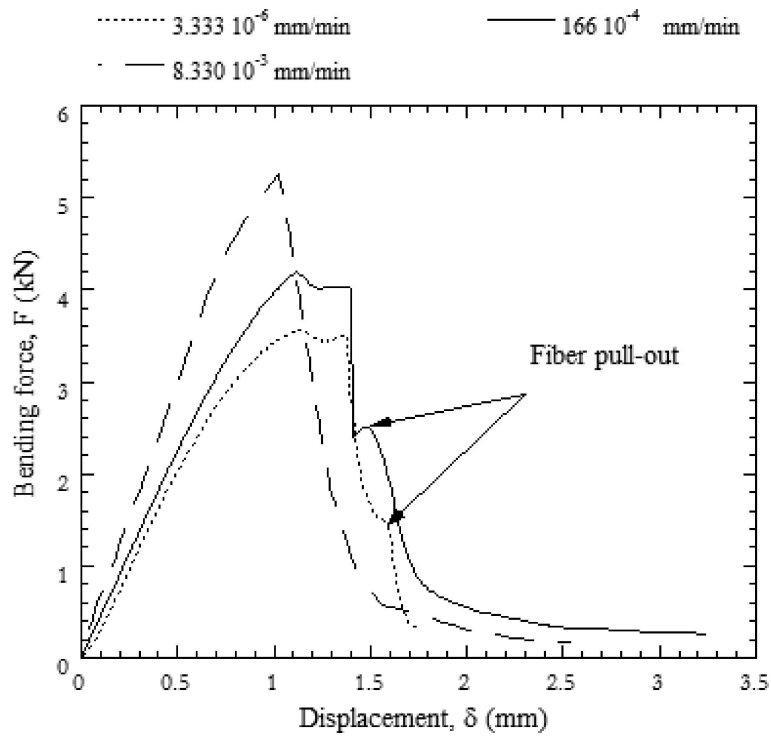
FIG. 3. Comparison of force-displacement curves for different
quasi-static displacement rates.
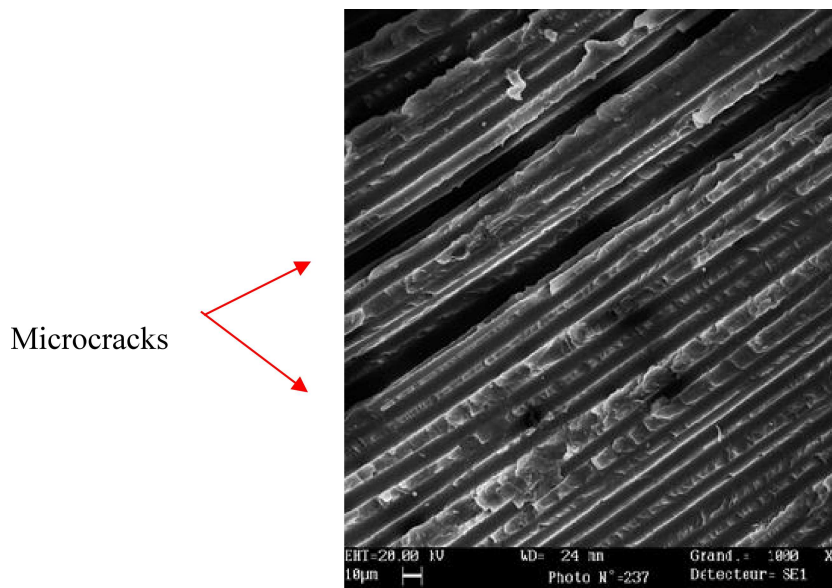
FIG. 4. Microcracks in the matrix close to the tensile face.
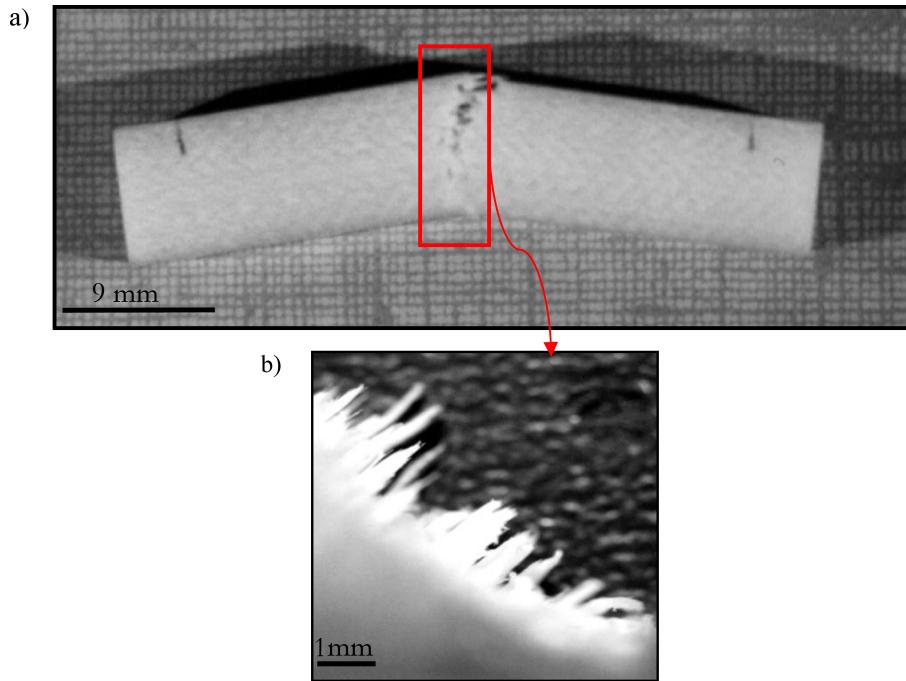
FIG. 5. a) Quasi-static rupture after three-point bending test, b) rupture face
of the specimen loaded by quasi-static three-point bending.

3.2. Dynamic bending

The dynamic bending tests have been carried out with the specimens obtained from the same plate and of the same geometry. Figure 6 shows a set of curves representing the forces calculated at supports as a function of the displacements measured at the central point of the specimen, the latter is calculated by Eqs. (2.2) and (2.4). The curves are given for different impact velocities.

It is noticed that the loading phase is accompanied by certain oscillations of variable amplitude, which are coming from the acceleration field.

The suppression of the force is related to the loss of contact between the support and the specimen. Therefore the rupture appears at "one-point bending" where the only resistance attributed to the specimen at this moment is its inertia [1]. It may be concluded that above the impact velocity of $V_4 = 38$ m/s, the vibrations become less important and the specimen is no longer losing contact with the supports.

In order to identify more precisely all the phenomena observed during the loading process over time, a dynamic analysis using a mass-spring model is proposed.
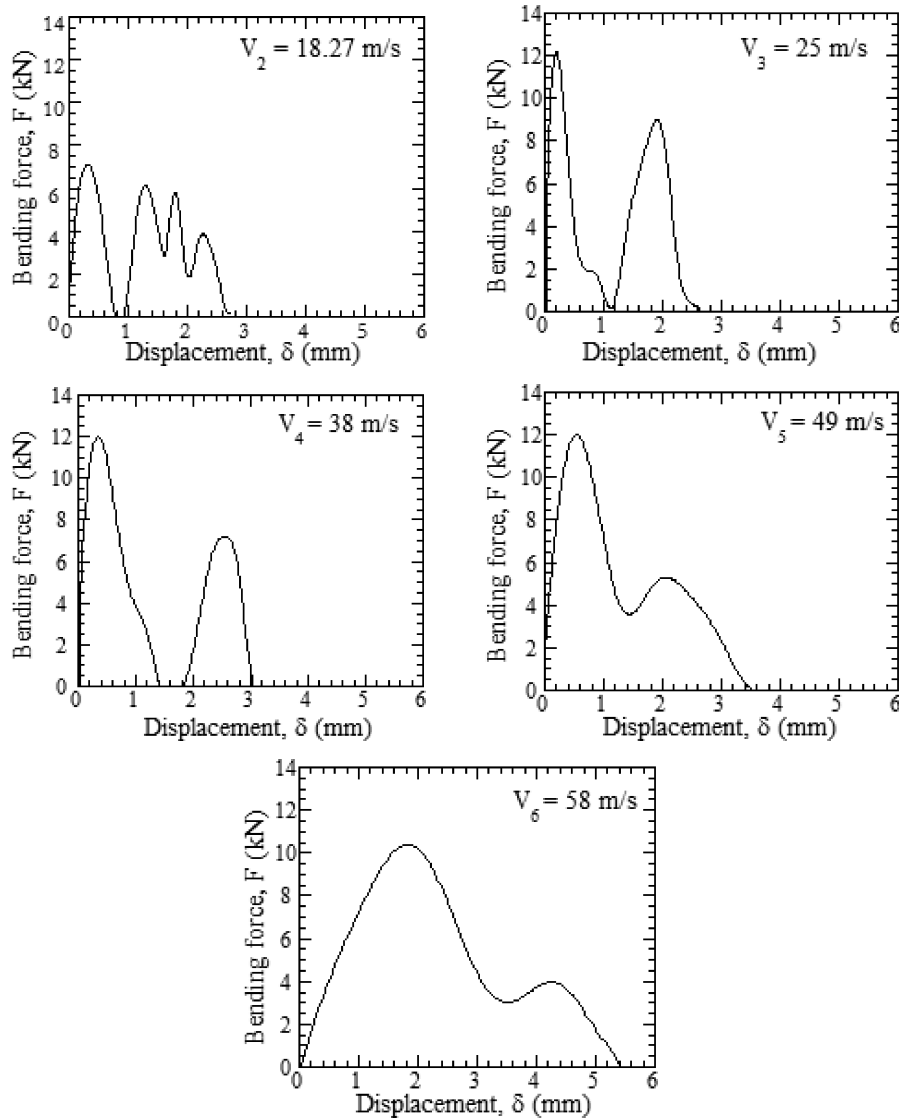
FIG. 6. Evolution of the transmitted force as a function of displacement
at different impact velocities.

4. ANALYSIS OF IMPACT TESTS

Many authors tried to model the three-point dynamic bending using the mass-spring model. The common problems were to estimate the stiffness values and the rigidity of the contact surface. The principal characteristic of such model is that no deformation localisation can be considered. Among the most impor-

tant models presented in the literature, the one by Williams [8–10] is adopted for the analysis. The principle is presented in Fig. 7.
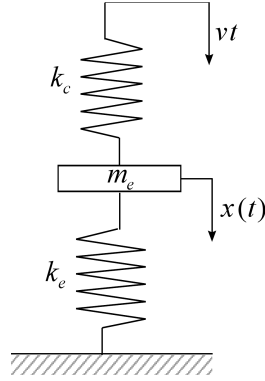
FIG. 7. Mechanical model representing behaviour of the impactor-specimen system during impact loading.

The system specimen-contact force is modelled by a spring of k_e stiffness, a corrected mass m_e and finally by another contact spring of k_c stiffness. The corrected mass m_e is assumed equal to 17/35 of the real specimen mass (WIL-LIAMS [8]).

The equation of movement is then as follows:

$$(4.1) \qquad m_e \ddot{x} + (k_c + k_e)x = k_c V_0 t.$$

If the initial conditions are $x(0) = \dot{x}(0) = 0$, the specimen displacement is given by

$$(4.2) \qquad x = \frac{\alpha}{\alpha + 1} \frac{V_0}{\omega} (\omega t - \sin(\omega t)),$$

where V_0 is the projectile velocity, $\alpha = \frac{k_c}{k_e}$ and $\omega^2 = \frac{k_c + k_e}{m_e}$ are the eigen pulsations of the system, which depend on the specimen dimensions B, W, S (see Fig. 1) and on the material density ρ.

The contact force is therefore obtained by the following:

$$(4.3) \qquad P_c = k_c(V_0 t - x) = \frac{\alpha}{\alpha + 1} k_e \frac{V_0}{\omega} (\omega t + \alpha \sin(\omega t)).$$

The force applied to the spring k_e is

$$(4.4) \qquad P_e = k_e x = \frac{\alpha}{\alpha + 1} k_e \frac{V_0}{\omega} (\omega t - \sin(\omega t)).$$

Equation (4.2) reproduces very well the oscillating behaviour of the specimen, the form of the displacement curve is the same as shown with experimental

results (Fig. 6). This encourages to use the Williams model for higher impact velocities.

The model allows to identify the rigidity during the shock tests. We will not calculate the contact rigidity of the projectile-specimen system from the contact law (Hertz theory), because the cylinder-plan contact is one of the most complex. However, a parametrical study may be a simple tool to estimate this rigidity from the force-time curves calculated at the point of impact. Once we know the rigidity and the specimen mass, we are able to estimate the value of the contact rigidity of the projectile-specimen system.

There are many formulas to calculate a value of C_e (inverse to the stiffness). For the homogenous isotropic material in the elastic range, this value for the specimens without notches can be deducted from the mid- displacement of the beam subjected to the three-point bending (KOBAYASHI [11]):

$$(4.5) \qquad C_e E B = \frac{S^3}{4W^3} \left(1 + 2.85 \left(\frac{W}{S} \right)^2 - 0.84 \left(\frac{W}{S} \right)^3 \right),$$

where E, B, W and S are, respectively, the Young modulus, the specimen width, the specimen thickness and the distance between supports (Fig. 1).

By using Eqs. (2.1), (2.4) and (2.6), we are able to calculate the force applied at the impact point of the specimen:

$$(4.6) \qquad F_I(t) = m_s \ddot{\delta}_{\text{ext}}(t) - m_s C_0 \varepsilon_T(t) + \left(\frac{\pi}{4} \left(D_{\text{ext}}^2 - D_{\text{int}}^2 \right) E_{tub} \varepsilon_{\text{T}}(t) \right).$$

Figure 8 represents a comparison of the force evolution as a function of time, both estimated from the model and calculated from Eq. (4.6). Two impact velocities are used for this comparison.
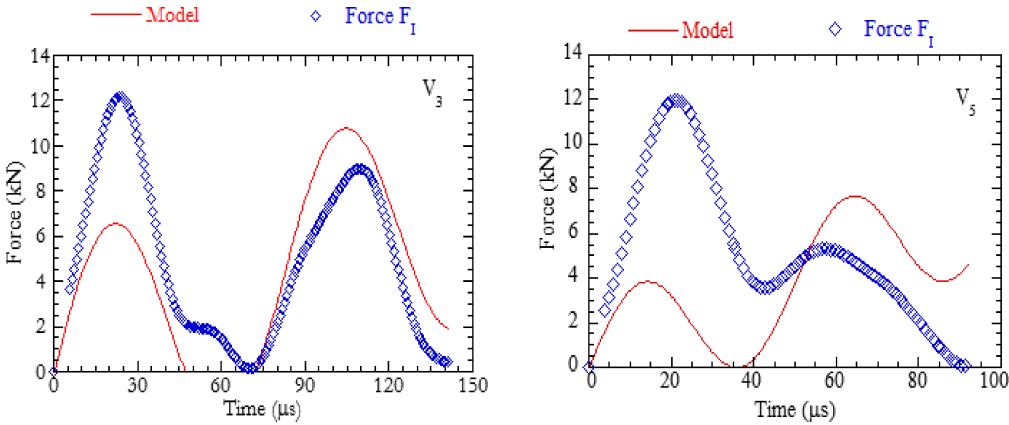
FIG. 8. Comparison between Williams model and equation; force is calculated at the impact point, the impact velocities are $V_3 = 25$ m/s and $V_5 = 49$ m/s.

The results obtained from the mass-spring model are presented in Table 2.

Table 2. Estimation of the test parameters from Williams model.

Impact velocity [m/s]	α	k_e [10^6 N/m]	ω [10^3 rad/s]	k_c [10^7 N/m]
$V_3 = 25$	6	4.06	76.47	2.40
$V_5 = 49$	7.5	4.06	77.56	3.04

Figure 8 clearly shows that the model reflects the phenomenon of the contact loss. In addition, the shapes of the force-time curves obtained from the model and from the tests are similar. On the other hand, the slopes of the force-time curves as well as the amplitudes are different. As far as the loading time is considered, both analytical and experimental results are very coherent.

Once we analyse the damaging process of the specimen, the model is less performing at high impact velocities. This behaviour can be explained by the modification of the contact rigidity (Table 2) during the rupture propagation [12]. This parameter plays a key role during the impact and it influences the inertial force.

In order to study the role of the acceleration field in the dynamic regime, we have introduced a correction factor γ which represents the effect of the acceleration field on the force applied at the central point of the specimen. If no acceleration effects are observed as it is under quasi-static loading, F_I is equal to F_T (Eq. (2.6)). However, in dynamics this factor is defined by the following relation:

$$(4.7) \qquad \gamma = \frac{F_T}{F_I}.$$

If equations (2.6), (4.2) and (4.3) are used, we can obtain the dynamic correction factor γ from the Williams model. Thus, we finally obtain the following expression:

$$(4.8) \qquad \gamma(\alpha, \xi) = 1 - \left(\frac{(\alpha + 1)\sin \xi}{\xi + (\alpha \sin \xi)} \right)$$

with $\xi = \omega t$.

Figures 9 and 10 represent the evolution of the dynamic correction factor γ as a function of time and for different values of α. The value $\gamma = 1$ corresponds to the quasi-static loading. The conclusion is that the dynamic effects are dominant when the specimen-projectile contact is too rigid. It should be noted that the Williams model neglects the rigidity of the specimen support system.

The curves presented in Fig. 10 clearly demonstrate the capacity of the Williams model to reproduce a phenomenon of the contact loss between the
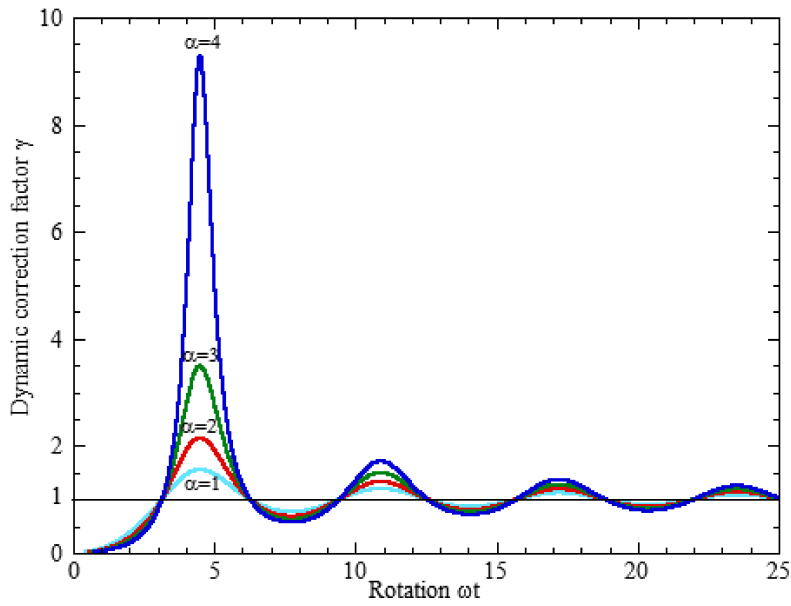
FIG. 9. Dynamic correction factor γ based on the Williams model
for different values of α.
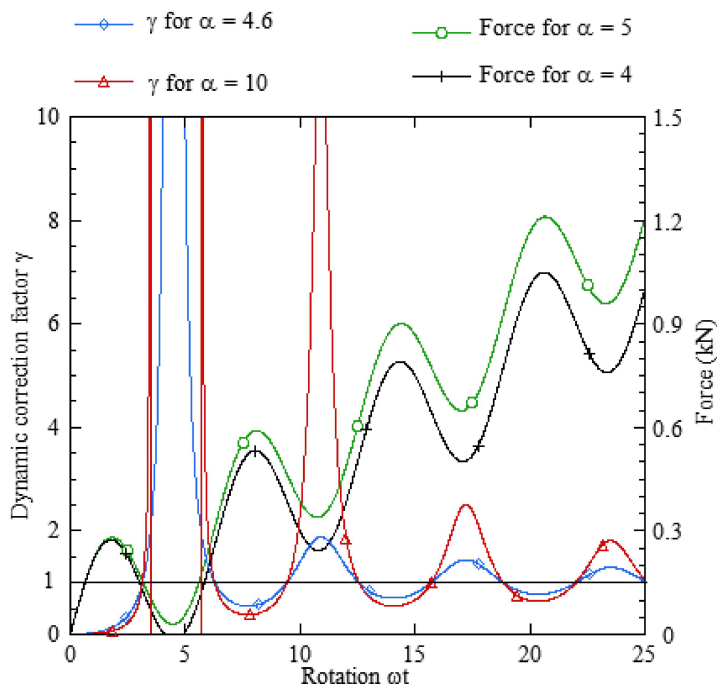
FIG. 10. Evolution of the dynamic correction factor γ as a function of time (Williams model);
$V_0 = 1$ m/s, $k_e = 4.055 \ 10^6$ N/m, $\omega = 80,000$ rad/s.

specimen and supports. This happens for the value of $\alpha \geq 5$. The same figure also confirms our experimental analysis by showing the importance of the dynamic effects at the moment of the contact loss.

We can notice that the model is better adopted for impacts with moderate velocities. In case of high impact velocities, the effects of inertia and the mechanisms of the irreversible absorption become too important and thus too perturbing.

5. EFFECT OF THE LOADING VELOCITY

In order to better understand the influence of the impact velocity on the specimen behaviour under the three-point bending test, we will analyse the changes in energy and stresses as a function of the impact velocity. Figure 11 shows an increase of the rupture stress as the impact velocity increases, up to a critical value comprised between 20 and 25 m/s. Above these values, we observe a decrease of the ultimate stress. This phenomenon has already been reported for composite materials with thermoplastic matrix by many authors [13]. It is attributed to the disappearance of the transition point between fragile and ductile rupture and, as a consequence, it leads to the decrease of the rupture stress value.
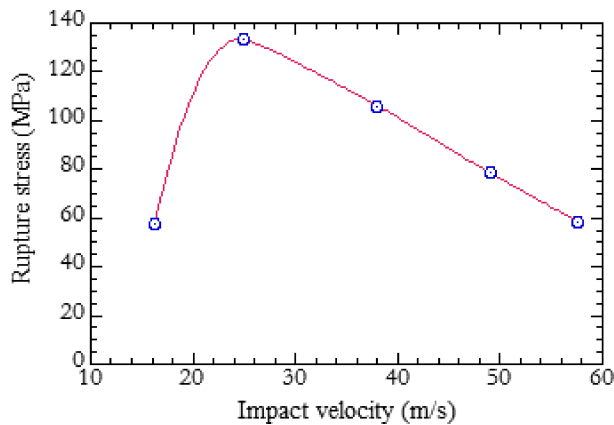
FIG. 11. Influence of the impact velocity on the rupture stress.

Evolution of the maximum force measured at supports during the first oscillation is given in Fig. 12 as a function of the impact velocity. This confirms a tendency of the material to change its rupture mode.

Figure 13 presents the change of the kinetic energy and deformation energy values as a function of time. Determination of the kinetic energy takes into account the inertia of the specimen rotation. The evolution of the deformation
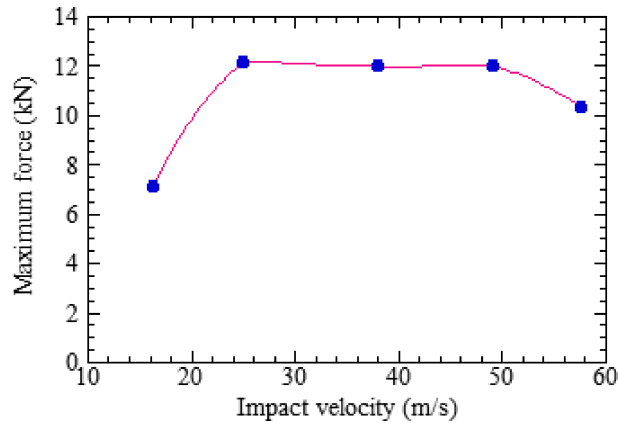
Fig. 12. Influence of the impact velocity on the rupture stress.
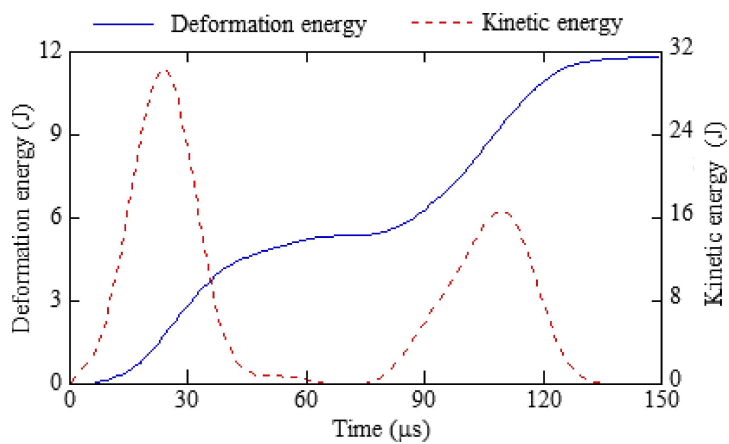
Fig. 13. Evolution of the kinetic and deformation energies
as a function of time.

energy produces a plateau for a short time interval comprised between 67 μs and 78 μs. Above these values, the contact of specimen-supports is re-established and the rupture continues to appear only due to the inertia efforts (the specimen is in the configuration "one-point bending").

Figure 14 presents the evolution of the total energy as a function of time, both are at quasi-static and dynamic ranges. It is observed that the total energy slightly increases when quasi-static loading velocity becomes higher. However, this total energy value becomes very sensible to the impact velocity once we reach the values of the order of 10 m/s. At the same time, the rupture stresses have a reverse tendency, i.e., they decrease (Fig. 11). This phenomenon can be explained by faster decrease of the displacement because the rupture itself

becomes more and more fragile, unless it reaches the point at which the phe-
nomenon is reversed and the rupture becomes more ductile.
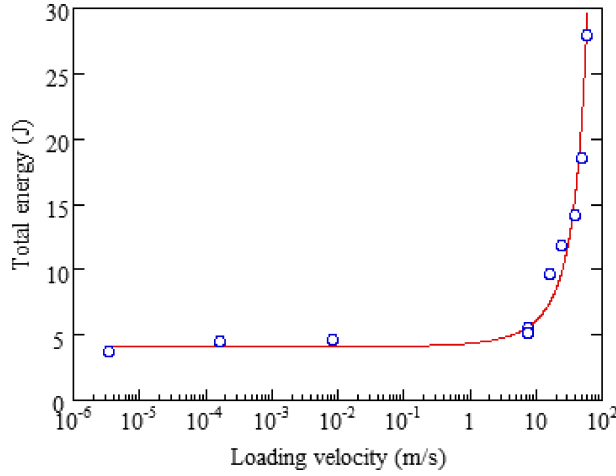
FIG. 14. Influence of the loading velocity on the total energy.

The displacement augments faster than the stress decreases and, as a conse-
quence, the total absorbed energy also increases.

These results allow to propose an exponential form of the correlation between
the total energy and the loading velocity. The proposed equation is

$$(5.1) \qquad W_T = \left(\frac{W_0}{2}\right)\left(1 + \exp\left(\left(\frac{V_i}{V_{i0}}\right)^m\right)\right),$$

where W_0 represents the total energy in quasi-static conditions, V_{i0} is the critical
velocity corresponding to the transition between the state of the insensibility and
the sensibility to the loading velocity and m is the coefficient of the sensibility to
the loading velocity. This expression can describe the behaviour of the composite
PA6 subjected to the three-point bending with the following constant values:
$W_0 = 4.1$ J, $V_{i0} = 16.8$ m/s and $m = 0.75$.

6. CONCLUSIONS

During the analysis of woven glass-fibre-reinforced Polyamide 6 behaviour
subjected to dynamic bending, a methodological approach has been proposed
based on two techniques: the mass-spring modelling and the experimental tech-
nique consisting of measurements of the force and displacement in order to find
the contact rigidity. Impact velocities in a range between 18.27 m/s and 58.0 m/s
have been proposed.

The use of the mass-spring model for moderate impact velocities remains an interesting tool to determine the effective load acting on the specimen. However, the identification of parameters at higher impact velocities is troublesome due to the fragility of PA6.

The existence of a critical impact velocity has been observed. Once this critical value is reached, the failure stress decreases quickly. The opposite behaviour, i.e., the increase of the rupture stress is observed while approaching the critical impact velocity. This behaviour can be explained by the existence of the transition between brittle and ductile rupture. Above this critical loading, the rigidity of PA6 starts to decrease. This overall behaviour reflects the apparition of first microcracks in the matrix, due to the failure of the fibres close to the tensile face of the specimen. This phenomenon characterises a rupture mode related to pure tension.

The test results under dynamic loading confirm the increase of the total energy absorbed compared to the quasi-static loading.

The current market imposes high standards of a proper characterization of the material properties; therefore the experienced use of the Hopkinson bar set is crucial. This is why, the methodology presented in this study has a big potential in the study of materials for industrial applications, especially in automotive industry.

References

1. MASSAQ A., RUSINEK A., KLÓSAK M., *New experimental technique for dynamic bending of composite materials*, Engineering Transactions, **62**(3): 269–289, 2014.

2. CHARPY G., *Essay on the metals impact bend test of notched bars*, Memory & Reports from the Society of Civil Engineers of France, 1901.

3. FAZAL A., FANCEY K.S., *Viscoelastically prestressed polymeric matrix composites – effects of test span and fibre volume fraction on Charpy impact characteristics*, Composites Part B: Engineering, **44**(1): 472–479, 2013.

4. HOPKINSON B., *A method of measuring the pressure produced in the detonation of explosives or by impact of bullet*, Philosophical Transactions A, **213**, pp. 437–456, 1914.

5. MASSAQ A., RUSINEK A., KLÓSAK M., *Method for determination of the dynamic elastic modulus for composite materials*, Engineering Transactions, **61**(4): 301–315, 2013.

6. KLEPACZKO J.R., *An experimental technique for shear testing at high and very high strain rates. The case of mild steel*, International Journal of Impact Engineering, **15**(1): 25–39, 1994.

7. KLEPACZKO J.R., MATYSIAK S.J., *Analysis of longitudinal impact on semi-infinite circular bars and tubes*, Appendix No 2, The Final Technical Report Contract DAJA 45-90-C-0052, Metz, October, 1992.

8. WILLIAMS J.G., ADAMS G.C., *The analysis of instrumented impact tests using a mass-spring model*, International Journal of Fracture, **33**(3): 209–222, 1987.

9. WILLIAMS J.G., *The analysis of dynamic fracture using lumped mass spring models*, International Journal of Fracture, **33**(1): 47–59, 1987.

10. WILLIAMS J.G., TROPSA V., MACGILLIVRAY H., RAGER A., *Dynamic correction factors for K and G in high rate, SENB, impact tests*, International Journal of Fracture, **107**(3): 259–278, 2001.

11. KOBAYASHI T., *Analysis of impact properties of 4533 steel for nuclear reactor pressure vessel by instrumented impact test*, Engineering Fracture Mechanics, **19**(1): 49–65, 1984.

12. EFFENDI R., *Failure mechanisms analysis under compression of unidirectional carbon/epoxy composites and micromechanical modeling*, PhD thesis, ENSAM, 1993.

13. GOLOVOY A., *Influence of velocity on the impact strength of glass reinforced polypropylene*, Polymer Composites, **7**(6): 405–412, 1986.

14. YOKOYAMA T., KISHIDA K., *A novel impact three-point bend test method for determining dynamic fracture-initiation toughness*, Experimental Mechanics, **29**(2): 188–194, 1989.

15. HANUS J.-L., MAGNAIN B., DURAND B., RODRIGUEZ J.A., BAILLY P., *Processing dynamic split Hopkinson three-point bending test with normalized specimen of quasi-brittle material*, Mechanics & Industry, **13**(6): 381–393, 2012.

16. JIANG F., VECCHIO K.S., *Hopkinson bar loaded fracture experimental technique: a critical review of dynamic fracture toughness tests*, Applied Mechanics Reviews, **62**(6): 060802-1–060802-39, 2009.

17. DELVARE F., HANUS J.-L., BAILLY P., *A non-equilibrium approach to processing Hopkinson bar bending test data: application to quasi-brittle materials*, International Journal of Impact Engineering, **37**(1): 1170–1179, 2010.

18. GOVENDER R.A., LANGDON G.S., NURICK G.N., CLOETE T.J., *Impact delamination testing of fibre reinforced polymers using Hopkinson pressure bars*, Engineering Fracture Mechanics, **101**: 80–90, 2013.

19. NAZARENKO E., *Fracture behavior of a ceramic fiber reinforced glass-ceramic matrix composite under both static and dynamic loadings*, PhD Thesis of the Ecole Centrale de Paris, 1992.

20. PIGNON A., MATHIEU G., RICHOMME S., MARGOT J.M., DELVARE F., *Modified split Hopkinson pressure bars for dynamic bending and shear tests*, Journal of Physics IV France, **134**: 725–730, 2006.